Helical Twist Senses, Liquid Crystalline Behavior, Crystal Microtwins, and Rotation Twins in a Polyester Containing Main-Chain Molecular Asymmetry and Effects of the Number of Methylene Units in the Backbones on the Phase Structures and Morphologies of Its Homologues

Xin Weng, Christopher Y. Li,† Shi Jin, Dong Zhang, John Z. Zhang, Feng Bai, Frank W. Harris, and Stephen Z. D. Cheng*

Maurice Morton Institute and Department of Polymer Science, The University of Akron, Akron, Ohio 44325-3909

Bernard Lotz

Charles Sadron of Macromolecules, 6 Rue Boussingault, Strasbourg 67083, France

Received August 30, 2002; Revised Manuscript Received October 17, 2002

ABSTRACT: A nonracemic chiral main-chain liquid crystalline (LC) polyester was synthesized from (*R*)-(−)-4′-{*ω*-[2-(*p*-hydroxy-*o*-nitrophenyloxy)-1-propyloxy]-1-undecyloxy}-4-biphenylcarboxylic acid via an A−B type condensation polymerization. The polymer was abbreviated as PET(R*-11), where 11 is the number of methylene units in the chain backbone. Other PETs(R*-*n*) ($n = 7-11$) in this series were also studied. PET(R*-11) exhibited a LC chiral smectic C (S_C*), a chiral smectic A (S_A*), and a twist grain boundary smectic A (TGBA*) phase with increasing temperatures as identified by differential scanning calorimetry, polarized light microscopy, and wide-angle X-ray diffraction (WAXD). Flat-elongated lamellae were observed in transmission electron microscopy (TEM) for thin-film melt crystallized samples. Its crystal structure was determined to be a monoclinic basic unit cell with $a = 1.03$ nm, $b = 0.47$ nm, $c = 6.43$ nm, and $\gamma = 83°$ via selected area electron diffraction (SAED), and these measurements were confirmed by two-dimensional WAXD fiber patterns. Furthermore, SAED results showed that two kinds of crystal twins existed in this polymer: "microtwinning" within one single lamellar crystal and "rotation-twinning" between two lamellae. This rotation-twinning was possibly a result of a mechanism of a soft epitaxy between two contacting folded surfaces along the {310} planes. Right-handed helical lamellar crystals were also found under the same crystallization conditions, and their pitch lengths were on the micrometer scale as observed by TEM and atomic force microscopy. The helical crystal structure was found to be identical to that of the flat-elongated counterparts. It was particularly surprising that in this series of PETs(R*-*n*) the odd−even methylene unit number effects existed on broad length scales. This included not only thermodynamic properties of the S_C* and the S_A* LC transitions but also the helical crystal handedness and the crystal structures.

Introduction

Chiral materials have been an extensively studied area in the field of materials science ever since the observation of their optical activity in the early nineteenth century.[1] Most applications of chiral systems are based on their unique properties, which are directly related to the atomic (configurational) chiral centers and helical conformations.[2−4] Therefore, manipulating the molecular design and subsequently transferring the chirality to macroscopic length scales is not only an important scientific issue but also a practical problem in technological applications.

Polymers with molecular asymmetry in their backbones are most widely observed in natural life forms. Biopolymers, such as DNA, collagen, and myosin, show precise control over their molecular helicity; i.e., the twist senses of their chiral structures are determined by the configuration of the chiral center in the nucleotide or peptide backbone.[5−7] In synthetic polymers, controlling the helical twist sense can be achieved by not only varying the molecular chirality but also via repeating units, hydrogen bonding, side chains, and block copolymers. In some cases, the helical twist senses can even be turned by environmental factors such as temperature, solvents, initiators, pH value, light, and salt concentrations.[8−15]

Liquid crystalline (LC) polymers make up a relatively new class of materials with special properties "in between" liquid crystals and polymers themselves.[16,17] When molecular chirality is introduced into LC polymers, chiral LC phases having helical morphology are induced, resulting in a series of potential applications in optics and electrooptics.[18−20] In chiral liquid crystals, helical morphologies with different handedness in the cholesteric and smectic C* (S_C*) phase have also been observed.[21,22] This morphology is often considered to be related to the configurational chirality. In some cases, such as in bent-core liquid crystals, the helical morphology is associated with shape of the mesogens and, therefore, the conformational asymmetry.[23] In biopolymers, a few examples have been observed in highly ordered crystalline phases; e.g., *Bombyx Mori fibroin* can grow helical crystals of the β modification with singularly handed helicity under solution crystallization conditions.[24] A quantitative understanding of the formation of the morphological chirality from the chirality influenced by the configurational and conformational

† Current address: Department of Materials Engineering, Drexel University, Philadelphia, PA, 19104. E-mail: chrisli@drexel.edu.

* To whom correspondence should be addressed. E-mail: scheng@uakron.edu.

10.1021/ma0214106 CCC: $22.00
Published on Web 11/21/2002

chirality has, however, not been completely understood.[25−30]

Recently, we reported that in a specially designed nonracemic chiral main-chain LC polyester synthesized from (*R*)-(−)-4′-{*ω*-[2-(*p*-hydroxy-*o*-nitrophenyloxy)-1-propyloxy]-1-nonyloxy}-4-biphenylcarboxylic acid [PET-(R*-9), containing nine methylene units in a repeating unit], helical single lamellar crystals, right-handed, were observed via isothermal crystallization.[31] The helical crystals possessed the identical structure and the chain-folding behavior as the flat-elongated lamellae prepared under the same crystallization conditions. Dark field experiments in transmission electron microscopy (TEM) have shown that the chain orientation in these helical crystals was twisted along two axes (double-twist),[32−35] similar to the structure in chromosomes.[36,37] This polymer also exhibited several chiral LC phases.[38]

To achieve a better understanding of the influence of molecular structure on the helical twist sense, two other polymers in this series, PET(S*-9) and PET(R*-10), were synthesized and studied. PET(S*-9) has the same repeating unit but an opposite configurational chiral center with respect to PET(R*-9), while PET(R*-10) possesses the identical chiral center but one more methylene unit in its repeating unit than PET(R*-9). Surprisingly enough, both PET(S*-9) and PET(R*-10) exhibited left-handed helical crystals, which was opposite to that of PET(R*-9).[39,40] This example shows that the number of methylene units also plays a vital role on the helical twist sense of the lamellar crystals.

In this publication, we report our recent study on the principle and mechanism of the effects of the number of methylene units on the helical crystal handedness and the LC and crystal structures of PET(R*-11), which has 11 methylene units in the polymer backbones. It is interesting that PET(R*-11) exhibits some different structural features from those of PET(R*-9 and 10). In particular, crystal microtwinnings and rotation-twinnings in two different length scales were observed in PET(R*-11). We also found that the odd and even numbers of methylene units in the polymer backbones had a profound effect on the structures, morphologies, and thermodynamic transition properties in this series of PET(R*-*n*) on much broader length scales compared with the classical understanding.

Experimental Section

Materials and Sample Preparation. PET(R*-11) was synthesized from (*R*)-(−)-4′-{*ω*-[2-(*p*-hydroxy-*o*-nitrophenyloxy)-1-propyloxy]-1-undecyloxy}-4-biphenylcarboxylic acid via an A−B type condensation polymerization. The detailed synthetic routes of the monomer and polymer are published elsewhere.[41] The configurations of the chiral centers in the backbones were R*. In this paper, the major investigation was focused on PET-(R*-11). However, other PETs(R*-*n*) with $n = 7-11$ were also used to distinguish the odd−even effect on structures, morphologies, and thermodynamic properties. In a general chemical structure form, the number of methylene units in this series of polymers is represented by *n*, and the degree of polymerization was *m*:

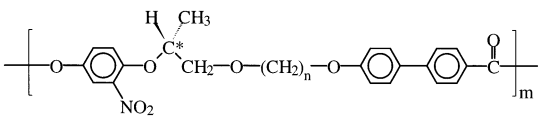

The number-average molecular weight of PET(R*-11) was 15 600 g/mol and the polydispersity was 1.78, as measured by gel permeation chromatography based on polystyrene standards. The characteristics of some PETs(R*-*n*) in this series were reported previously.[31−35,38−40] Their number-average molecular weights were between 10 000 and 40 000 g/mol, and polydispersities were between 1.7 and 2.3.

For one-dimensional (1D) wide-angle X-ray diffraction (WAXD) powder measurements, thick film samples (∼0.1 mm) were prepared via a melting press. Fiber samples spun from the S_A* LC phase were used in 2D WAXD fiber experiments to determine the phase structures. The samples used in polarized light microscopy (PLM) observations were melt-processed between two glass slides with a typical thickness of 10 μm. Polymer thin films (with a thickness of 50−100 nm) were prepared via solution casting from a 0.05% (w/v) tetrahydrofuran solution. After the solvent was evaporated, the samples were ready for TEM and atomic force microscopy (AFM) experiments.

Equipment and Experiments. The thermal behaviors of the phase transitions were studied with a Perkin-Elmer DSC-7. The temperatures and heat flows at different cooling and heating rates were calibrated using standard materials. To eliminate the thermal history, the samples were first heated to above the isotropic temperature. The cooling experiments always preceded the heating experiments, and the cooling and heating rates were always kept identical. The transition temperatures were determined by measuring the onset and peak temperatures from both the cooling and heating scans at different rates.

Reflection 1D WAXD powder experiments for obtaining structural change information were performed with a Rigaku 12 kW rotating anode X-ray (Cu Kα radiation) generator equipped with a diffractometer. The diffraction peak positions and widths were calibrated with silicon crystals of known crystal size in the high-2θ angle region and silver behenate in the low-2θ angle region. A sample hot stage was coupled to the diffractometer in order to study the polymer structural evolution with temperature during heating and cooling. The temperatures of this hot stage were calibrated to be within ±1 °C. Samples were scanned in a 2θ angle range between 1.5° and 35° with a scanning rate of 4°/min. Fiber 2D WAXD patterns were obtained using a Rigaku X-ray imaging system with an 18 kW rotating anode X-ray generator. A hot stage was also used to measure the elevated temperatures. A 30 min exposure time was required for a high-quality pattern. In both 1D and 2D WAXD experiments, background scattering was also subtracted from the sample scans.

Optical textures of the polymers were observed with a PLM (Olympus BH-2) coupled with a Mettler heating stage (FP-90). The films were heated in the stage to 175 °C, which was above the samples isotropic temperature, for 3 min, then quenched to preset temperatures, and held isothermally for various time periods ranging from one to several days under a dry nitrogen atmosphere. The morphological textures were then recorded.

A morphological study on the nanometer scale was carried out in a JEOL (1200 EX II) TEM using an accelerating voltage of 120 kV. The thin film samples had identical thermal treatments as those used for PLM experiments, but the samples were subsequently quenched into liquid nitrogen and allowed to return to room temperature (note that the glass transition temperature, T_g, of this polymer is at 32 °C). Then they were shadowed by Pt and coated with carbon for TEM morphological observations. Selected area electron diffraction (SAED) patterns of the samples having different zones were obtained using a tilting stage to determine the crystal unit-cell symmetry and dimensions. The smallest aperture was used with a diameter of ∼0.5 μm to study the SAED patterns of the helical crystals, which is within the half pitch length of the crystals. The camera length was set at 50 cm, and the calibration of the ED spacing was performed using the TlCl *d*-spacings and their multiples.

For the AFM experiments, the same thin film samples were used directly without the shadowing and coating performed for the TEM study. An AFM (Digital Instrument Nanoscope IIIa) with a J-scanner was also used to examine the crystal

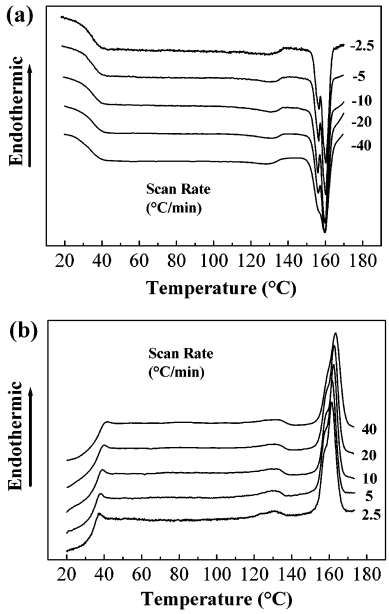

Figure 1. Two sets of DSC cooling and heating thermographs of PET(R*-11) at different rates from 2.5 to 40 °C/min.

surface morphology. The force used by the cantilever was light enough to avoid damaging the sample, yet it was strong enough to obtain accurate surface features. The scanning rate was 1−2 Hz for the scan size of 5−25 μm. The scanner was calibrated with the standard grid in both lateral size and height.

The polyethylene (PE) decoration method was utilized to study the chain-folding direction of the lamellar crystals.[42,43] In this study, a linear PE fraction (number-average MW 17 000 g/mol and polydispersity 1.1) was used as the decoration material. During the decoration, an optimal 10 cm distance between the sample and the basket was chosen in the vacuum evaporator where PE was degraded and evaporated. The samples were then treated following the procedure as described previously.[42,43]

Results and Discussion

Phase Transitions and Their Structural Evolutions. Figure 1 shows two sets of DSC cooling and heating thermodiagrams at different rates ranging between 2.5 and 40 °C/min. The sudden change in the heat capacity at 32 °C in this figure indicates the T_g of PET(R*-11). At a temperature near 163 °C, two partially overlapped transitions could be observed. The latent heats of the two transitions are 3.64 and 1.29 kJ/mol, respectively. A small transition can be found at 130 °C with a transition enthalpy of 0.52 kJ/mol. The onset transition temperatures and heats of transitions exhibit very little heating or cooling rate dependence. This indicates that these transitions are close to thermodynamic equilibrium, and they may be associated with low ordered LC transformations.

Figure 2 shows a set of 1D WAXD powder patterns during cooling at 2.5 °C/min. At temperatures above 170 °C, the polymer was in the isotropic melt (I), and only an amorphous halo at $2\theta = 18.6°$ could be observed. This corresponds to a liquidlike, short-range order in molecular lateral packing. When the temperature reached 163 °C, a low-angle diffraction at $2\theta = 2.85°$ developed, which usually indicates the formation of the layer structure of a smectic LC phase. The temperature at which this diffraction appeared also corresponds to an observation of a sudden narrowing of the width at half-height of the scattering halo (Figure 3a). Therefore, this

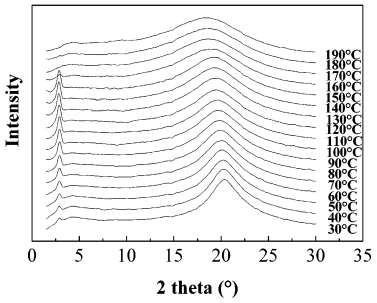

Figure 2. Set of WAXD powder patterns of PET(R*-11) during cooling at 2.5 °C/min.

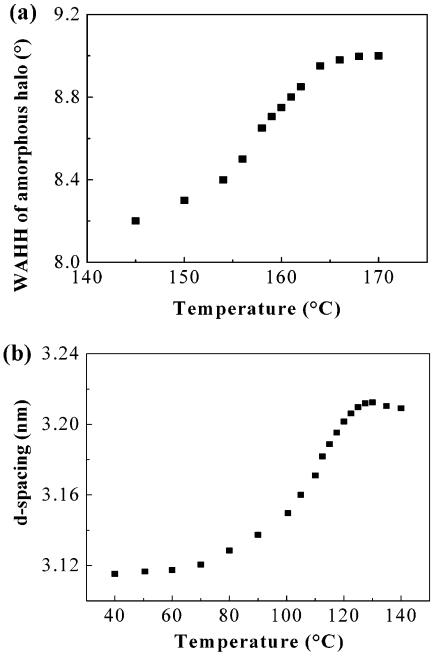

Figure 3. Changes of width at half-height of the scattering halo in the WAXD powder patterns with temperature (a) and changes of *d*-spacing of the low-angle WAXD powder pattern peak with temperature (b).

reflects an increase in the correlation length of the molecular lateral packing in the LC state. As the temperature decreased further, the high-angle scattering halo continuously but slightly shifted to larger 2θ angles due to the thermal shrinkage. The *d*-spacing change of the low-angle diffraction with temperature is shown in Figure 3b. Only at temperatures below 130 °C did the *d*-spacing start to decrease drastically. This reveals a transition corresponding to the small transition observed in the DSC thermodiagrams at 130 °C (Figure 1). The rapid decrease of the *d*-spacing below 130 °C was attributed to a molecular chain tilting in undergoing a second-order or at least a weak first-order transition to form another smectic phase (most likely, a S_C* phase; see below). The WAXD patterns during heating were identical to those during cooling in Figure 2.

Determination of the Low Ordered LC Phases. To identify structures of the low-ordered smectic LC phases in PET(R*-11), 2D WAXD fiber patterns taken at 100 and 140 °C are shown in parts a and b of Figure 4, respectively. At 100 °C, two pairs of the low-2θ angle layer diffractions are tilted ±29° to the meridian, and the high-2θ angle scattering halos are on the equator. This indicates a S_C* phase with the molecular chains parallel and the layer normal tilted ±29° to the fiber

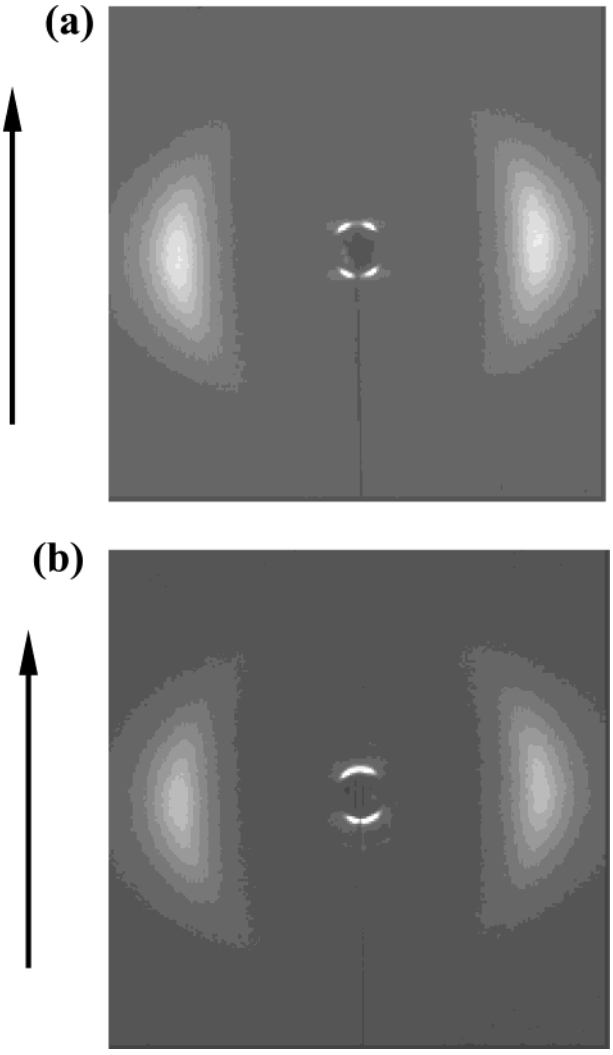

Figure 4. 2D WAXD fiber patterns the S_C* phase at 100 °C (a) and the S_A* phase at 140 °C (b). The arrow direction is the fiber direction.

direction (note that the WAXD fiber pattern of a S_C* phase is identical to a S_C phase). When the fiber was heated to 140 °C, the two pairs of the low-2θ angle layer diffractions in the quadrants merged into one pair located on the meridian, while the pair of high-2θ angle scattering halos remained on the equator (Figure 4b). This is the characteristics of a S_A* phase. On the basis of these 2D WAXD results, the small transition at 130 °C was identified as a S_A* ↔ S_C* phase transition.

These phase assignments are also supported by the optical textures observed in PLM. When the polymer was held at 100 °C, a broken focal conic texture of the S_C* phase was seen as shown in Figure 5a. The dark broken lines may also represent the pitch of the S_C* helices. This transformed into the focal conic texture of S_A* phase without broken lines at 140 °C (Figure 5b), since broken lines are commonly generated by a large tilting angle of the chains from the S_A* to the S_C* phases (here is ±29°). When the temperature was increased further to 160 °C, the texture changed as shown in Figure 5c, which can be classified as the optical filament texture of TGBA* phase.[38,44] In this phase, which is observed in a narrow temperature region, the smectic layer structure represented by the low-angle diffraction remained as observed in the 1D WAXD patterns in Figure 2. By slowly heating the sample to 162 °C in

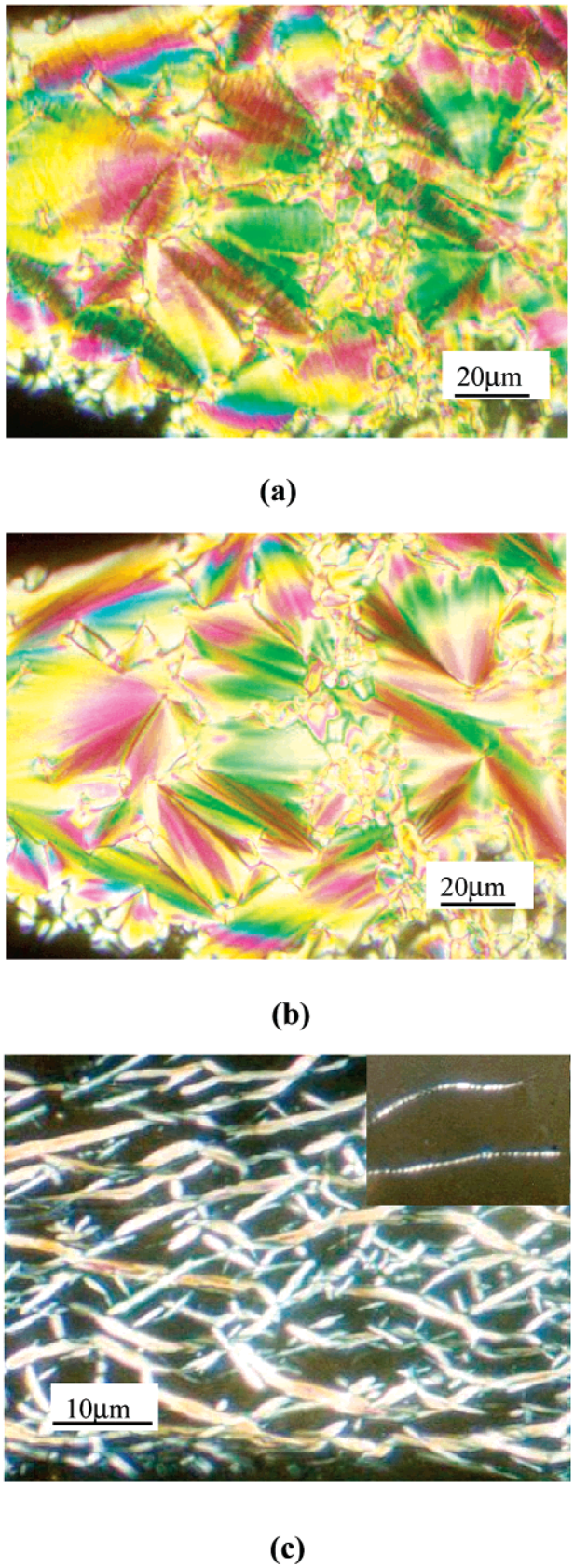

Figure 5. PLM morphological micrographs of the broken focal conic texture of S_C* phase at 100 °C (a), the focal conic texture of S_A* phase at 140 °C (b), and the filament texture of TGBA phase at 160 °C with an inset of the remaining filament texture of the TGBA phase at 162 °C (c).

PLM, which is only 1 °C lower than the isotropic temperature, a few elongated filaments were still bire-

fringent. An alternation of strong and weak birefringence along the filaments' long axis was on the micrometer scale, which represents a periodic change of molecular orientation in a helical arrangement (inset of Figure 5c). In the DSC results, this narrow temperature TGBA* phase was between the S_A* phase and the isotropic melt between 158 and 163 °C.

Structural Determination of the Flat-Elongated Lamellar Crystals. As seen in the DSC results (Figure 1), no crystallization, even at a cooling rate as slow as 2.5 °C/min, was observed. This indicates that even if PET(R*-11) is able to crystallize, its kinetics must be very slow. By prolonging the isothermal crystallization time, lamellar crystals could indeed grow in a temperature range between 100 and 150 °C (note that the crystallization can occur in both the S_A* and the S_C* phases). Figure 6a is a TEM micrograph of a flat-elongated lamellar crystal of PET(R*-11) grown at 135 °C for 1 day in the S_A* phase. The shape of the crystal was largely anisotropic, indicating the anisotropy of crystal growth rates along the long and short axes of this crystal. Figure 6b shows a flat-elongated lamellar crystal after PE oligomer decoration. The PE crystal rods appeared to be perpendicular to the long axis. Since the PE chains are perpendicular to the long axis of the PE rods, the chain-folding direction of this elongated lamellar crystal must be along the long axis of the crystal.[42,43]

The thickness of the lamellar crystal in Figure 6a was around 40 nm, based on the metal shadowing size measured in TEM. A number of TEM and AFM images show that single crystal lamellar thickness is generally around 13−28 nm, depending upon crystallization temperatures. For the lamellae crystallized under the same conditions, however, the overall thickness may vary substantially as a result of multiple lamellar stacking. Figure 7a shows a [00*l*] zone SAED pattern of the flat-elongated lamellar crystal, from which the *a***b** plane information can be obtained (the *c* axis is parallel to the *c** axis). The *a** axis is defined in the horizontal direction of the ED pattern (corresponding to the short axis of the lamella in the real space), and the *a* dimension can be calculated from the (200) diffraction ($a = 1.03$ nm). At the $^1/_3$ distance between the neighboring strong diffraction layers parallel to the *a** axis, a weak diffraction layer can also be seen that may be attributed to a superstructure in the crystal.[31−35,38] By combining both of the strong (*h*10) and (*h*00) diffractions, we speculate the structure as being a construction of two identical ED patterns overlapped together in a mirror image along the *b* axis. The SAED pattern in Figure 7a can then be viewed as two identical basic unit cells with a twin relationship (see below). This basic unit cell is monoclinic with $b = 0.47$ nm based on the (010) diffraction, and the γ is 83°.

Tilting experiments were conducted to determine the *c* axis dimension of the unit cell. Figure 7b,c shows two SAED patterns with different zones by tilting the crystal around the $\underline{b}$ axis (the long axis) to generate the $[10\bar{1}]$ and the $[20\bar{1}]$ zones. From this, the *c* axis dimension of the unit cell was determined to be 6.43 nm. Considering that the calculated repeating unit length with all-trans methylene units is about 3.25 nm, this *c* axis dimension represents a nearly extended (zigzag) conformation of the chain stems in the crystal, and each unit cell has the length of two chemical repeat units. Therefore, the basic monoclinic unit cell structure has $a = 1.03$ nm, $b = 0.47$ nm, $c = 6.43$ nm, $\alpha = \beta = 90°$, and $\gamma = 83°$.

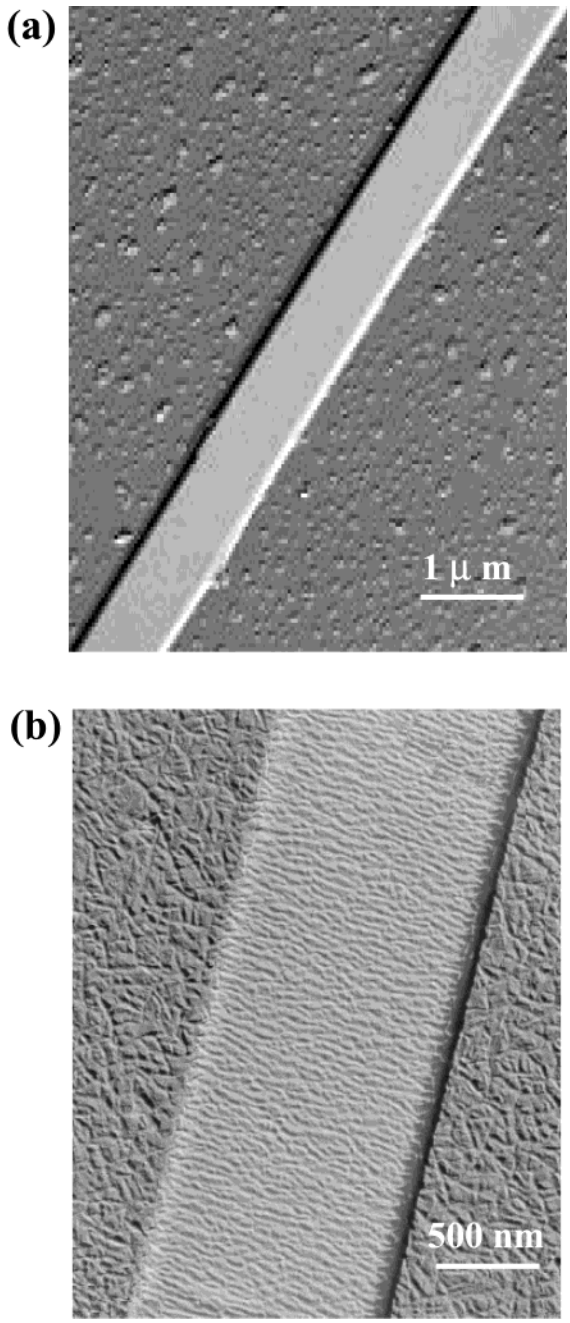

Figure 6. A flat-elongated lamellar crystal of PET(R*-11) (a) and a PE oligomer decorated flat-elongated lamellar crystal (b).

This crystal structure was also confirmed using 2D WAXD fiber pattern as shown in Figure 8. The sample was annealed at 100 °C for 10 days at a constant length condition. Sharp, intense (00*l*) diffractions were found on the meridian, indicating that the molecule chain was along the fiber direction. The (200) and (110) diffractions were found on the equator, and the (10*l*), (20*l*), and (205) diffractions appeared in quadrants. All the *d*-spacings of these diffractions were in good agreement with the observed and calculated data based on the unit cell dimensions determined via SAED results.

Crystal Twinning on Two Different Length Scales. As described previously, Figure 7a exhibits a twin structure, and the twin planes were parallel to the *b* axis, as shown in Figure 9. This kind of (100) microtwinned crystal structure is unique for this series

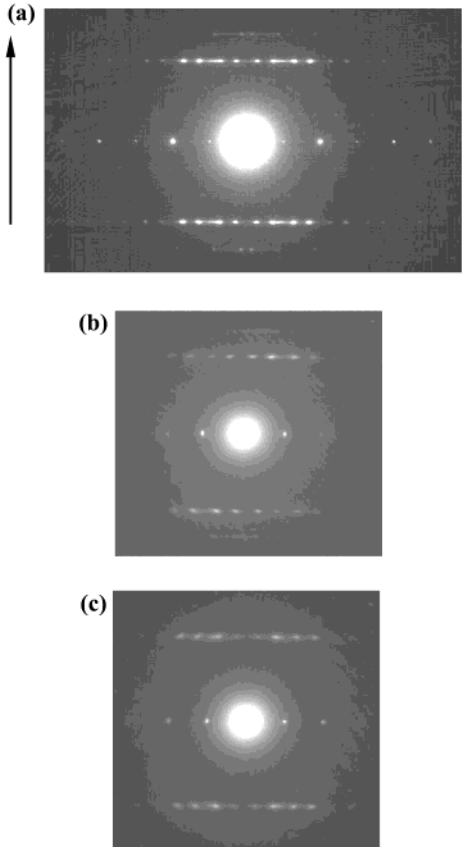

Figure 7. SAED pattern of a flat-elongated lamellar crystal obtained from Figure 6a; the arrow direction corresponds to the long axis of the lamella in the real space (a). SAED pattern obtained by tilting around the *b* axis about ±9° to show the [10$\bar{1}$] zone (b) and ±17° to show the [20$\bar{1}$] zone (c). Note that they are microtwins, and therefore, both clockwise and counterclockwise rotation generate identical results.

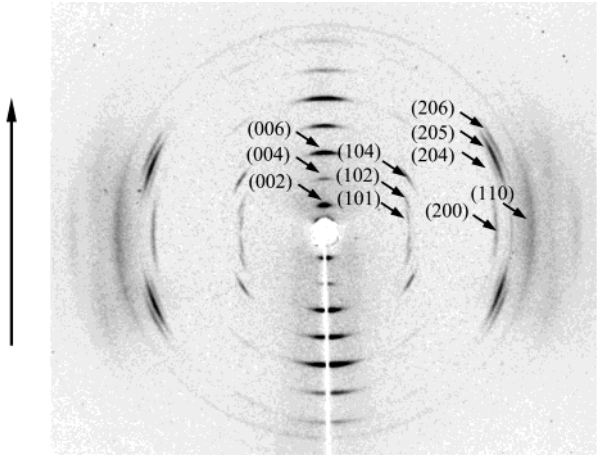

Figure 8. 2D WAXD fiber pattern of sheared sample and then annealed at 100 °C for 10 days. The arrow direction is the shear direction.

of polymers since the twinning occurred on a nanometer length scale and the number of twin planes in the crystal was large. Detailed molecular arrangement of twin structures of this kind is not known. Computer simulation is currently being undertaken to understand how this kind of twin structures can be constructed.

Under the same crystallization condition, lamellae with a lozenge shape were sometimes observed as shown in Figure 10a. The *acute* angle in the lozenge crystal was characteristically 34°. A SAED pattern obtained

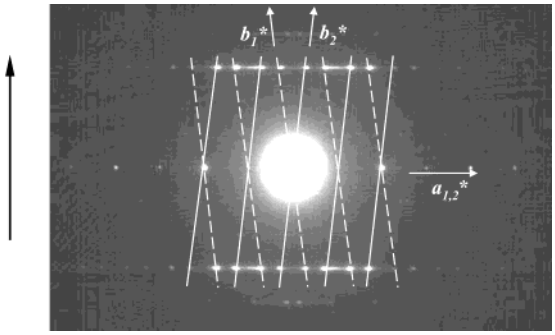

Figure 9. Resolved twin structure of the pattern in Figure 7a, which consists of two sets of diffractions with *a** and *b** axes indicated in the figure, and the twin plane is along the *b* axis.

from this crystal (inserted in Figure 10a) showed that the pattern was actually composed of two sets of the SAED patterns (as shown in Figure 7a) superimposed together, and they had an angle of 34° between two *b* axes in these two crystals. This indicates that the observed lozenge crystal must possess another type of twin structure that is superimposed on the "microtwinning". This twin structure is referred as a "macrotwinning" on the micrometer length scale. To study the nature of this twin structure, PE crystal rods after the PE oligomer decoration experiment showed that a single orientation was observed on the lamellar crystal surface. This orientation was perpendicular to one pair of the lamellar edges (parallel to the b_2 axis) and tilted 34° with respect to another pair (the b_1 axis, Figure 10a). This indicates that the crystal in this figure must have two completely superimposed lamellar crystals on top of one another (note that the b_1 axis belongs to the bottom lamellar layer).

This prediction can be proven by the observation in Figure 10b. In this figure, PE crystal rods after the PE oligomer decoration reveal that the rod orientation was different on the top and bottom lamellar folded surfaces (enlarged micrograph, see Figure 10c). On each lamellar folded surface, PE crystal rods were perpendicular to their own *b* axis (the pair of edges of the crystal). Therefore, it is speculated that for the crystals in Figure 10a the top and bottom lamellae started to grow at the same time, and they always superimpose on one another. The shape of the twin crystal was a lozenge because of confinements in growth brought to each other. For the crystals in Figure 10b, the bottom lamella grew first, and the top one then followed. Therefore, the growth of the top lamellar crystal lagged, and it was also confined by the elongated geometry of the bottom lamella. The final elongated morphology of the twin crystals was along the *b* axis of the bottom lamella, resulting with the still exposed part of the bottom lamella exhibiting its own PE crystal rod orientation.

This kind of twin structure can be identified as a rotation-twin crystallography; i.e., one lamella can be generated by rotating another lamella 180° around the bisector, which serves as a 2_1 screw axis.[45,46] Another type of rotation-twin structure has been found in the lamellar branching ("quadrites") of the α form of isotactic polypropylene (it-PP).[47] In that case, the a_1 and c_1 axes of the radial lamella are parallel to the c_2 and a_2 of the tangential one. Therefore, both lamellae have a common *b* axis, and their contact plane is the (010). Because of the interaction of the helices of different stem handedness in it-PP, the branching takes place when-

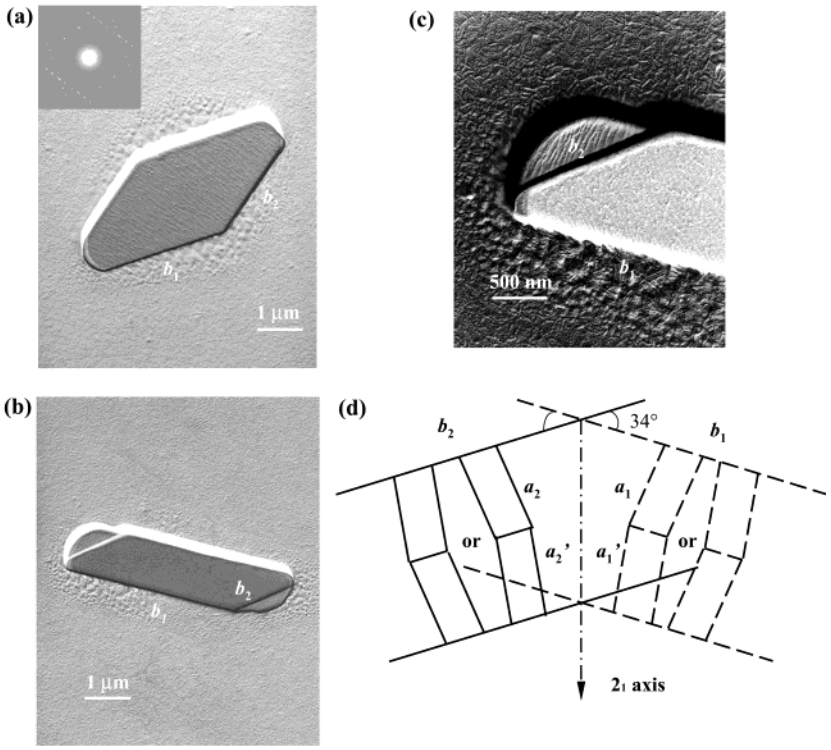

Figure 10. TEM micrograph of a "macrotwin" lamella (decorated with PE oligomers), the inset being the SAED pattern of the crystal (a); an elongated "macrotwin" lamellae (decorated with the PE oligomers) (b); the tip of the crystals in (b) (c); and schematic drawing of rotational twin: the bottom lamella is shown by dashed line and the top by the solid line. By rotating the bottom lamella around the 2_1 axis (bisector), the top lamella can be obtained (d).

ever two successive *ac* layers are made of the same stem handedness; however, the crystallographic unit cell requires that they be of opposite handedness.[47]

In our case, the contact plane of the top and bottom lamellae is the chain-folding plane. Therefore, we speculate that this is associated with the "soft" epitaxy of the chain folds on two different lamellar contact folded surfaces. When the folding direction of the top microtwinned lamella, that is along its *b* axis, can be aligned along one of the $\{\bar{3}10\}$ planes of the bottom microtwinned lamella, a 34° angle between two *b* axes of these lamellae can be generated (see Figure 10d). To have this soft epitaxy, the folds on the contact surface of the bottom lamella must have regular arrangements along the *b* axis, and the folds of the top lamella are along one of the $\{\bar{3}10\}$ planes of the bottom lamella. However, the existence of the microtwin may further complicate this rotation-twin. Quantitative analyses are currently under investigation.

Morphology and Structure of Helical Lamellar Crystals and Their Odd−Even Effect in Different Length Scales. As in the case of PET(R*-9)[31] under the same crystallization condition where flat-elongated lamellar crystals grew, helical lamellar crystals could also form as shown in Figure 11a. The inset SAED pattern obtained from the helical crystal within the half pitch length of the helical crystal was identical to the flat-elongated crystals with more diffuse streaks indicating that the helical crystals also possessed the microtwinning monoclinic cells. Decorated PE crystal rods on the helical crystal surface were perpendicular to the long helical axis, revealing that the chain-folding direction was also along the *b* axis of the crystal. Figure 11b is the AFM image of a right-handed helical crystal, and the pitch length of this crystal was about 2 μm. Therefore, the handedness of PET(R*-11) helical crystal was identical to that of PET(R*-9), but opposite to that of PET(R*-10).[31−35,39]

This observation clearly indicates that the molecular chirality is important, but not the only factor to consider in determining the chirality on the large length scales. We have previously demonstrated that the chirality transformation is determined most critically by *the pack scheme of the building blocks on each structural length scales*.[39] With regard to the effect of methylene units on the helical twist sense, it was reported that helical handedness varies with both configuration of asymmetric carbon and the number of carbon atoms in the alkyl tails from the aromatic center core in the cholesteric (Ch) LC phase of small molecules.[48] This rule, with some modifications, also extends to the S_C* phase, including the direction of self-polarization.[49,50] Based on this rule, the Ch and S_C* phases in the LC homologues exhibit morphological helicity that is affected by the number of methylene units in the tails. Namely, the molecules with odd numbers of methylene units have an opposite handedness as those with even numbers of methylene units. This effect was attributed to the molecular conformation differences between these two sets of LC homologues, although specific structural packing schemes were not determined. Theoretical and simulational studies in predicting the helical twist sense of LC homologues were extensively pursued.[51−54]

After examining this series of PET(R*-*n*) ($n = 7-11$), we observed profound odd−even effects in different length scales. (The detailed studies of PET(R*-7) and PET(R*-8) are undertaken.) This effect was found not only on the helical handedness as we just described but also from crystal unit cell length scale to thermodynamic transition properties. In the unit cell length scale, the PETs(R*-odd) possessed monoclinic cells with a *c* axis having a length of two chemical repeating units,[55] while

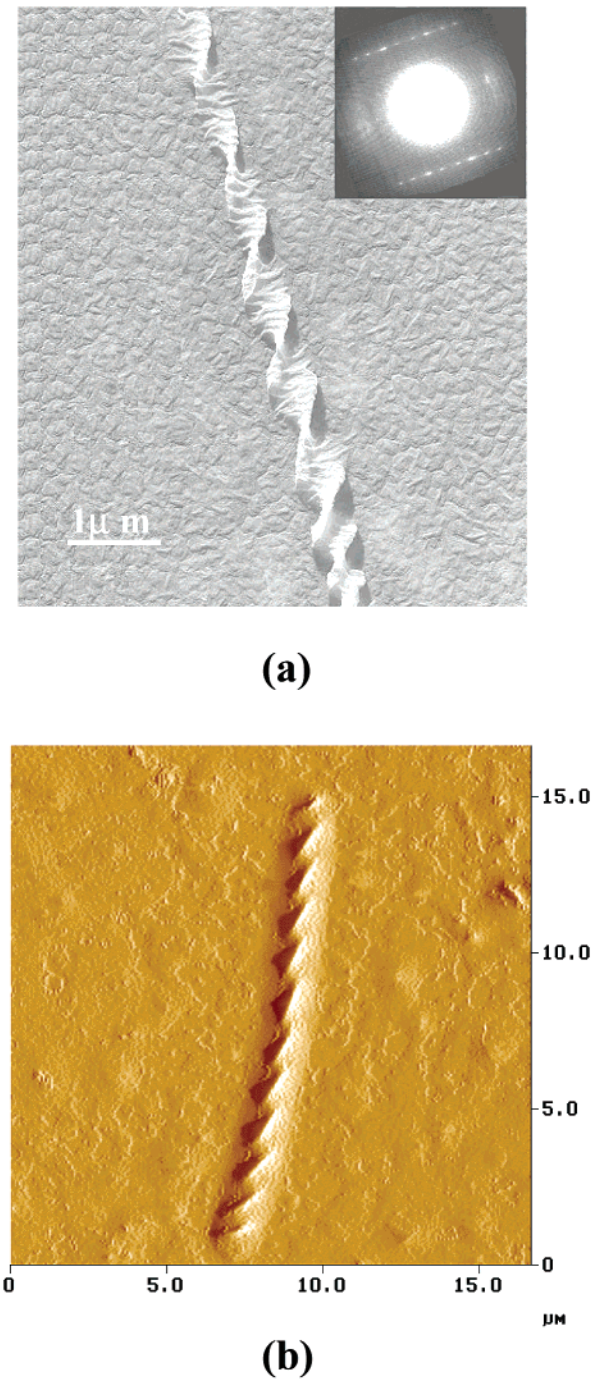

Figure 11. TEM micrograph of PET(R*-11) helical lamellar crystal grown at 135 °C; the inset is the SAED pattern of the helical crystal using the smallest aperture (a). AFM tapping mode image of a helical lamellar crystal (b).

PETs(R*-even) had orthorhombic cells with a *c* axis length of one repeating unit. The odd−even effects on thermodynamic transition properties are shown in Figure 12a,b, which include the S_C^* ↔ S_A^*, S_A^* ↔ TGBA*, and TGBA* ↔ I phase transitions.[56] Figure 12a clearly indicates that the LC phase transitions of PETs(R*-odd) are lower compared with those of PETs(R*-even), and this odd−even effect is stronger in the S_C^* phase than those in the S_A^* and TGBA* phases. In Figure 12b, the heats of transitions of the S_C^* ↔ S_A^* and the S_A^* ↔ TGBA* also exhibit identical trends. However, this effect is much stronger in the transition of S_C^* ↔ S_A^* than that in the S_A^* ↔ TGBA* transition.

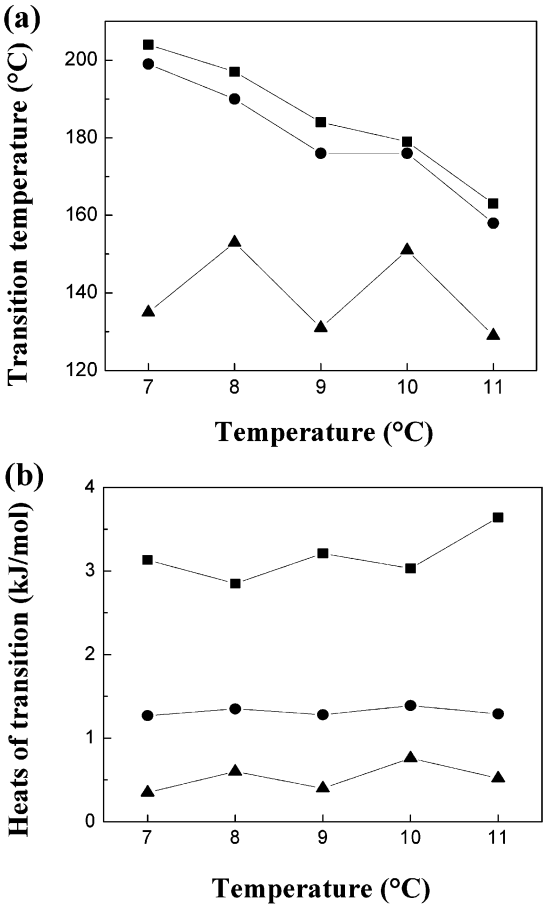

Figure 12. Odd−even effects of the LC phase transition temperatures (a) and heats of transitions for PET(R*-*n*)s (b): ▲, S_C^* ↔ S_A^*; ●, S_A^* ↔ TGBA*; ■, TGBA* ↔ I.

Surprisingly enough, in the TGBA* ↔ I transitions, the heats of transitions of PETs(R*-odd) are higher than those of PETs(R*-even), which does not follow the trends of the other odd−even effect for the rest of the transitions. The reason for this abnormal behavior of the odd−even effect is not clear at this moment. We expect that this may be associated with the total atom number of the spacers in the backbones of the polymers and their different packing.

Conclusion

In summary, phase structures, transition behaviors, and crystal morphologies of PET(R*-11) have been investigated. This chiral polyester exhibits the S_C^*, S_A^*, and TGBA* LC phases. Flat-elongated lamellar crystals have been observed after prolonged crystallization times in both of the S_A^* and S_C^* phases. The crystal structure possessed a basic monoclinic unit cells with dimensions of $a = 1.03$ nm, $b = 0.47$ nm, $c = 64.3$ nm, and $\gamma = 83°$. Under the same crystallization conditions, right-handed helical lamellar crystals were also observed, and they had the same crystal structure as the flat-elongated ones. It is particularly interesting that two crystal twin forms could be identified: the microtwinning on the nanometer length scale and the rotation-twinning on a micrometer scale. In the rotation-twin crystals, two lamellar crystals were stacked on top of each other. There was a 34° rotation between the two *b* axes of the top and bottom lamellae which shared the common *c* axis. A possible soft epitaxy mechanism in forming this rotation-twin was proposed. It has also been found that

the odd−even effect, caused by the number of methylene units in the backbones in this PET(R*-*n*) series, affected not only the LC phase transition temperatures and heats of transitions but also the crystal structures, dimensions, and the handedness of helical lamellar crystals.

Acknowledgment. This work was supported by the NSF (DMR-0203994) and the ALCOM Scientific and Technology Center (DMR-91-57738) at Kent State University, Case Western Reserve University, and the University of Akron. The authors are also grateful to Dr. Freddy Khoury for his valuable and extensive discussions on the topic of structure and twinning.

References and Notes

(1) Silverman, M. P. *Waves and Grains: Reflections on Light and Learning*; Princeton University Press: Princeton, 1998.
(2) Schadt, M.; Helfrich, W. *Appl. Phys. Lett.* **1971**, *18*, 127.
(3) Meyer, R. B.; Liebert, L.; Strzelecki, L.; Keller, P. *J. Phys., Lett.* **1975**, *36*, L69.
(4) Clark, N. A.; Lagerwell, S. T. *Appl. Phys. Lett.* **1980**, *36*, 899.
(5) Dickerson, R. E.; Drew, H. R.; Conner, B. N.; Wing, R. M.; Fratini, A. V.; Kopka, M. L. *Science* **1982**, *216*, 475.
(6) Okuyama, K.; Arnott, S.; Takanyanagi, M.; Kakudo, M. *J. Mol. Biol.* **1981**, *152*, 427.
(7) Warrick, H. M.; Spudish, J. A. *Annu. Rev. Cell Biol.* **1987**, *3*, 379.
(8) Fujiki, M. *J. Am. Chem. Soc.* **2000**, *122*, 3336.
(9) Nelson, J. C.; Saven, J. G.; Moore, J. S.; Wolynes, P. G. *Science* **1997**, *277*, 1793.
(10) Prince, R. B.; Saven, J. G.; Wolynes, P. G.; Moore, J. S. *J. Am. Chem. Soc.* **1999**, *121*, 3114.
(11) Blout, E. R.; Carver, J. P.; Gross, J. *J. Am. Chem. Soc.* **1963**, *85*, 644.
(12) Yashima, E.; Maeda, Y.; Okamoto, Y. *J. Am. Chem. Soc.* **1998**, *120*, 8895.
(13) Watanabe, J.; Okamoto, S.; Satoh, K.; Sakajiri, K.; Furuya, H. *Macromolecules* **1996**, *29*, 7084.
(14) Cheon, K. S.; Selinger, J. V.; Green, M. M. *Angew. Chem., Int. Ed.* **2000**, *39*, 1482.
(15) Takei, F.; Koichi, K.; Onitsuka, K.; Takahashi, S. *Angew. Chem., Int. Ed. Engl.* **1996**, *35*, 1554.
(16) Donald, A. M.; Windle, A. H. *Liquid Crystalline Polymers*, Cambridge University Press: Cambridge, 1992.
(17) Collyer, A. A. *Liquid Crystal Polymers: from structure to applications*; Elsevier Applied Science: Amsterdam, 1992.
(18) Tsutusui, T.; Tanaka, R. *Polymer* **1981**, *2*, 117.
(19) Hikmet, R. A. M.; Zwerver, B. H. *Liq. Cryst.* **1993**, *13*, 561.
(20) Lagerwell, S. T. *Liq. Cryst. Today* **1993**, *3*, 3.
(21) Slaney, A. J.; Nishiyama, I.; Styring, P.; Goodby, J. W. *J. Mater. Chem.* **1992**, *2*, 805.
(22) Styring, P.; Vuilk, J. D.; Nishiyama, I.; Slaney, A. J.; Goodby, J. W. *J. Mater. Chem.* **1993**, *3*, 399.
(23) Link, D. R.; Natale, G.; Shao, R.; Maclennan, J. E.; Clark, N. A.; Krblova, E.; Walba, D. M. *Science* **1997**, *278*, 1924.
(24) Lotz, B.; Vassal, A. G.; Brack, A.; Magoshi, J. *J. Mol. Biol.* **1982**, *156*, 345.
(25) Kaspar, M.; Gorecka, E.; Sverenyak, H.; Hamplova, V.; Glogarova, M.; Pakhomov, S. A. *Liq. Cryst.* **1995**, *19*, 589.
(26) Fuhrhop, J. H.; Helfrich, W. *Chem. Rev.* **1993**, *93*, 1565.
(27) Sakurai, I.; Karvamura, T.; Dakurai, A.; Kegami, A.; Setoi, T. *Mol. Cryst. Liq. Cryst.* **1985**, *130*, 203.
(28) Nandi, N.; Bagchi, B. *J. Am. Chem. Soc.* **1996**, *118*, 11208.
(29) Nandi, N.; Bagchi, B. *J. Phys. Chem. A* **1997**, *101*, 1343.
(30) Kruger, P.; Losche, M. *Phys. Rev. E* **2000**, *62*, 7031.
(31) Li, C. Y.; Yan, D.; Cheng, S. Z. D.; Bai, F.; Ge, J. J.; He, T.; Chien, L. C.; Harris, F. W.; Lotz, B. *Macromolecules* **1999**, *32*, 524.
(32) Li, C. Y.; Yan, D.; Cheng, S. Z. D.; Bai, F.; Ge, J. J.; He, T.; Chien, L. C.; Harris, F. W.; Lotz, B. *Phys. Rev. B* **1999**, *60*, 12675.
(33) Li, C. Y.; Cheng, S. Z. D.; Ge, J. J.; Bai, F.; Zhang, J. Z.; Mann, I. K.; Harris, F. W.; Chien, L. C.; Yan, D.; He, T.; Lotz, B. *Phys. Rev. Lett.* **1999**, *83*, 4558.
(34) Li, C. Y.; Cheng, S. Z. D.; Weng, X.; Ge, J. J.; Bai, F.; Zhang, J. Z.; Calhoun, B. H.; Harris, F. W.; Chien, L.-C.; Lotz, B. *J. Am. Chem. Soc.* **2000**, *122*, 73.
(35) Li, C. Y.; Ge, J. J.; Bai, F.; Calhoun, B. H.; Harris, F. W.; Cheng, S. Z. D.; Chien, L. C.; Lotz, B.; Keith, H. D. *Macromolecules* **2001**, *34*, 3634.
(36) Livolant, F.; Bouligand, Y. *Chromosoma* **1980**, *80*, 97.
(37) Kleman, M. *Adv. Phys.* **1989**, *38*, 605.
(38) Li, C. Y.; Ge, J. J.; Bai, F.; Zhang, J. Z.; Calhoun, B. H.; Chien, L. C.; Harris, F. W.; Cheng, S. Z. D. *Polymer* **2000**, *41*, 8953.
(39) Li, C. Y.; Cheng, S. Z. D.; Weng, X.; Ge, J. J.; Bai, F.; Zhang, J. Z.; Calhoun, B. H.; Harris, F. W.; Chien, L.-C.; Lotz, B. *J. Am. Chem. Soc.* **2001**, *123*, 2462.
(40) Li, C. Y.; Jin, S.; Weng, X.; Ge, J. J.; Zhang, D.; Bai, F.; Harris, F. W.; Cheng, S. Z. D.; Yan D.; He, T.; Lotz, B.; Chien, L.-C. *Macromolecules* **2002**, *35*, 5475.
(41) Bai, F.; Chien, L. C.; Li, C. Y.; Cheng, S. Z. D.; Percheck, R. *Chem. Mater.* **1999**, *11*, 1666.
(42) Wittmann, J. C.; Lotz, B. *Makromol. Rapid Commun.* **1982**, *3*, 733.
(43) Wittmann, J. C.; Lotz, B. *J. Polym. Sci., Polym. Phys. Ed.* **1985**, *23*, 205.
(44) Goodby, J. W.; Waugh, M. A.; Stein, S. M.; Chin, E.; Pindak, R.; Patel, J. S. *Nature (London)* **1989**, *337*, 449.
(45) Khoury, F.; Padden, F. J. Jr. *J. Polym. Sci.* **1960**, *47*, 455.
(46) Khoury, F. *J. Appl. Phys.* **1963**, *34*, **73.**
(47) Lotz, B.; Wittmann, J. C. *J. Polym. Sci., Polym. Phys.* **1986**, *24*, 1541.
(48) Gray, G. W.; McDonnell, D. G. *Mol. Cryst. Liq. Cryst. Lett.* **1977**, *34*, 211.
(49) Goodby, J. W.; Chin, E.; Leslie, T. M.; Geary, J. M.; Patel, J. S. *J. Am. Chem. Soc.* **1986**, *108*, 4729.
(50) Goodby, J. W.; Chin, E. J. S. *J. Am. Chem. Soc.* **1986**, *108*, 7424.
(51) Beresnev, L. A.; Blinov, L. M.; Osipov, M. A.; Pikin, S. A. *Mol. Cryst. Liq. Cryst.* **1988**, *158*, 3.
(52) Osipov, M. A.; Meister, R.; Stegemeyer, H. *Liq. Cryst.* **1994**, *16*, 173.
(53) Stegemeyer, H.; Sprick, A.; Osipov, M. A.; Vill, V.; Tunger, H. W. *Phys. Rev. E* **1995**, *51*, 5721.
(54) Emelyanenko, A. V.; Osipov, M. A.; Dunmur, D. A. *Phys. Rev. E* **2000**, *62*, 2340.
(55) For PET(R*-9), we have reported that the crystal structure is orthorhombic if we consider the rest of the ED spots belonging to a commensurate superstructure.[31] However, if we consider these diffractions to be attributed to the basic crystal structure, it is also possible to assign a monoclinic unit cell with a microtwinning, although this polymer possesses less precisely determined diffraction positions and intensities.
(56) For PET(R*10), the TGBA* phase only shows up under the cooling and heating rates which are extremely slow (e.g., at 0.5 °C/min).

MA0214106